Size analysis of nanocrystals in semiconductor doped silicate glasses with anomalous small-angle x ray and Raman scattering

G. Irmer[a] and J. Monecke
Institute of Theoretical Physics, Freiberg University of Mining and Technology, Bernhard-von-Cotta-Strasse 4, 09596 Freiberg, Germany

P. Verma
Department of Electronics and Information Science, Kyoto Institute of Technology, Kyoto 606-8585, Japan

G. Goerigk
DESY-HASYLAB, Notkestrasse 85, 22603 Hamburg, Germany

M. Herms
Fraunhofer-Institut für Zerstörungsfreie Prüfverfahren, Krügerstrasse 22, 01326 Dresden, Germany

(Received 14 February 2000; accepted for publication 2 May 2000)

Semiconductor doped glasses containing CdS_xSe_{1-x} nanocrystallites embedded in a silicate glass matrix were investigated. The dimensions of the nanocrystallites are in the range of a few nanometers and vary as a function of a secondary heat treatment. The confinement of such quantum dots for elementary excitations depends strongly on their size. In order to obtain a mean particle size and the size distribution, anomalous small angle x-ray scattering (ASAXS) and low-frequency inelastic Raman scattering measurements were performed. The sizes and the size distributions were evaluated for samples of different mean crystallite radius and composition *x*. The results of Raman measurements agree well with those of ASAXS, if both the acoustic mode damping across the nanocrystallite–matrix interface and the particle size distribution are taken into account in the Raman band shape analysis. The concentration of nanocrystallites in the glass matrix was determined by using the technique of contrast variation. Scattering curves were recorded at three energies below but close to the *K*-absorption edge of selenium (12.66 keV) and at 9.64 keV for comparison, which is significantly below the absorption edge. © *2000 American Institute of Physics.* [S0021-8979(00)08515-7]

I. INTRODUCTION

The optical properties of semiconducting crystallites with sizes of a few nanometers differ considerably from those of the corresponding bulk material. Such quantum dots are attractive for the study of the confinement, for instance, of excitons and phonons. Their physical properties strongly depend on the size distribution. Therefore, it is important to pay special attention to accurate comparative measurements of size and size distribution by different methods. In the past few years, special attention has been paid to CdS and CdS_xSe_{1-x} nanocrystallites grown in a silicate glass matrix by a special heat treatment. The use of such semiconductor doped glasses as sharp cutoff optical filters has been known for a long time. Applications as nonlinear optical material and in the field of integrated optics are under discussion.[1] The nanoparticles being nearly spherical shaped have been proven to be ideal model systems for the study of three-dimensional confinement. In previous works, high-resolution transmission electron microscopy,[2] small-angle x-ray scattering,[2–4] and Raman scattering[2,5–17] have been employed for the particle size analysis in semiconductor doped glasses. The technique of anomalous small-angle x-ray scattering (ASAXS) was introduced to the examination of these materials by Ref. 4. In this work, we compare results of ASAXS and Raman scattering measurements on the same samples, which contain CdS_xSe_{1-x} nanoparticles embedded in a glass matrix. The average diameters of the particles observed in different samples were in the range of 4–13 nm. The scattering curves (intensity vs wave vector) of the ASAXS measurements were fitted with different size distribution functions. The best fit results were achieved for asymmetric distribution functions with a pronounced density tail for particles smaller than the mean size. Further, the particle size was determined by Raman scattering based on the fact that the frequency of confined acoustic phonons is inversely proportional to the particle diameter. It is shown that the particle size is overestimated if the calculation uses only the maximum of the observed Raman peak as it has been frequently done in previous works. The wave vectors of bulk acoustic phonons are large in comparison to those of the exciting and the scattered light, but the observation of the acoustic modes in small particles is possible due to the uncertainty of the wave vector transferred in the Raman scattering process. The Raman intensity of the strongest acoustic mode with index $l=0$ shows the predicted dependence on the vibrational frequency. For calibration, the Boson peak of the glass matrix[6,18,19] in the Raman spectra at about 50 cm^{-1} can be used. The density of nanocrystallites in the glass ma-

[a]Author to whom correspondence should be addressed; electronic mail: irmer@physik.tu-freiberg.de

TABLE I. Anomalous-dispersion corrections for Cd, S, Se, Si, and O.

E (keV)	f'_{Cd}	f''_{Cd}	f'_{S}	f''_{S}	f'_{Se}	f''_{Se}	f'_{Si}	f''_{Si}	f'_{O}	f''_{O}
9.486	−0.138	3.517	0.268	0.409	−1.247	0.846	0.196	0.240	0.033	0.023
12.511	−0.450	2.174	0.186	0.240	−4.040	0.510	0.127	0.139	0.017	0.013
12.652	−0.477	2.132	0.183	0.234	−7.407	0.500	0.124	0.135	0.016	0.012
12.658	−0.478	2.130	0.183	0.234	−10.878	3.844	0.124	0.135	0.016	0.012

trix was obtained by ASAXS measurements with different x-ray energies close to the absorption edge of Se.

II. THEORY

A. Anomalous small-angle x-ray scattering

The ASAXS measurements were analyzed within a two-phase model: widely separated single-crystalline CdS_xSe_{1-x} spherical particles of radius R are embedded in a glass matrix mainly consisting of amorphous SiO_2. Since it was anticipated that the semiconducting nanoparticles occupy only a small volume fraction of the sample, one can assume that there are no particle correlation effects.

For N_p particles of equal volume $V_p=4\pi R^3/3$ distributed in the scattering volume V, the scattered cross section is given by[4,20]

$$\frac{d\sigma}{d\Omega}(q,E)=N_p(\Delta\rho)^2V_p^2S(q,R). \tag{1}$$

The contrast $\Delta\rho$ between the particle phase p and the matrix m depends on the x-ray energy E and is defined by

$$\Delta\rho(E)=|n_pF_p(E)-n_mF_m(E)|, \tag{2}$$

where $F_p(F_m)$ and $n_p(n_m)$ are the scattering factors and densities of CdS_xSe_{1-x} complexes (matrix molecules), respectively.

The scattering function $S(q,R)$ of a sphere with radius R is

$$S(q,R)=\left[\frac{3j_1(qR)}{(qR)}\right]^2, \tag{3}$$

where $j_1(x)=(\sin x-x\cos x)/x^2$ is the spherical Bessel function of first order. The scattering vector $\boldsymbol{q}$ has the magnitude $q=|\boldsymbol{q}|=(4\pi/\lambda)\sin\vartheta$, λ and 2ϑ being the x-ray wavelength and the scattering angle, respectively.

Equation (1) can be normalized to the number of matrix molecules n_mV in the scattering volume and the normalized cross section can be given as

$$\frac{d\tilde{\sigma}}{d\Omega}(q,E)=v_fn_m|\eta F_p(E)-F_m(E)|^2V_pS(q,R), \tag{4}$$

where $v_f=N_pV_p/V$ is the volume fraction of the CdS_xSe_{1-x} particles and $\eta=n_p/n_m$ is the ratio of molecule densities in the particle and the matrix phase, respectively.

Now we take into account that the particle size is not uniform. For a size distribution $c(R)$ the mean Radius $\overline{R}$ and mean volume $\overline{V}_p$ for nanoparticles are obtained from

$$\overline{R}=\int_0^\infty Rc(R)dR, \quad \overline{V}_p=(4\pi/3)\int_0^\infty R^3c(R)dR, \tag{5}$$

with $\int_0^\infty c(R)dR=1$.

Equation (4) should be replaced by

$$\frac{d\tilde{\sigma}}{d\Omega}(q,E)=v_fn_m|\eta F_p(E)-F_m(E)|^2(1/\overline{V}_p)\times\int V_p^2(R)c(R)S(q,R)dR, \tag{6}$$

with $v_f=N_p\overline{V}_p/N$.

The dependence of the scattered cross section on the x-ray energy E can be used to analyze the scattering contrast. The dispersion of the atomic scattering factors $f(E)$, which has a strong energy dependence close to the x-ray absorption edge, can be given as

$$f(E)=f^0+f'(E)+if''(E), \tag{7}$$

with f^0 being the number of electrons in the atom ($f^0_{Cd}=48$, $f^0_S=16$, $f^0_{Se}=34$, $f^0_{Si}=14$, and $f^0_0=8$) and f' and f'' being the so-called anomalous dispersion correction. The molecular scattering factors $F_p(E)$ and $F_m(E)$ are composed of the atomic scattering factors according to the stoichiometric composition of the particle and the matrix, respectively, and are given as

$$\begin{aligned}F_p(E)&=F'_p+iF''_p=f_{Cd}+xf_S+(1-x)f_{Se},\\ F_m(E)&=F'_m+iF''_m=f_{Si}+2f_0+\text{smaller ingredients.}\end{aligned} \tag{8}$$

Considering the scattered cross section at $q=0$, we get $S(0,R)=1$, and by use of Eq. (6) it follows that

$$\frac{d\tilde{\sigma}}{d\Omega}(0,E)=v_fn_m|\eta F_p(E)-F_m(E)|^2\overline{V}_pA, \tag{9}$$

with $A=(1/\overline{V}_p)^2\int V_p^2(R)c(R)dR$. As shown in Ref. 4, a linear approximation for the square root of the scattered cross section can be applied. The ratio η of the molecular densities in the particle and in the matrix is obtained from a fit procedure using the measured cross sections at different energies. In the vicinity of the K-absorption edge of Se (see Table I), the atomic scattering factors are mainly influenced by f'_{Se}.

The volume fraction v_f of the particles can be calculated using the integrated cross section of the scattering curve $(d\tilde{\sigma}/d\Omega)(q)$. By integration of Eq. (6) we obtain

$$v_f=\int\frac{d\tilde{\sigma}}{d\Omega}(q,E)d^3q\cdot[8\pi^3n_m|\eta F_p-F_m|^2]^{-1}, \tag{10}$$

which is independent of the particle size distribution. If the size distribution is known, for instance by a fit of the scattering curve $(d\tilde{\sigma}/d\Omega)(q,E)$, v_f can also be calculated from Eq. (9) using the value of the scattered cross section at $q=0$, as

$$v_f=\frac{d\tilde{\sigma}}{d\Omega}(0,E)[n_m|\eta F_p-F_m|^2\overline{V}_pA]^{-1}. \tag{11}$$

B. Raman scattering

In the low-frequency range of the Raman spectra, peaks of frequencies being inversely proportional to the diameter of the particles appear.[12] These frequencies correspond to the acoustic vibrations of the nanoparticles. The eigenfrequencies classified according to the symmetry group of a sphere are divided into two categories: torsional and spheroidal.

As shown by Duval,[21] only the spheroidal modes with angular quantum numbers $l=0$ and 2 are Raman active. The total symmetric mode $l=0$ is polarized and the quadrupolar symmetric mode $l=2$ is depolarized.

The vibrational frequencies are obtained from solutions of eigenvalue equations, which in the special case $l=0$, are given by[22]

$$\sin(\xi)=4\alpha^2 j_1(\xi). \tag{12}$$

The eigenvalues ξ_{lp} have a second index $p\,(=1,2,3,...)$ which distinguishes the lowest order mode $(p=1)$ from its overtones $(p\geqslant 1)$ in the Raman spectra. The eigenvalues determine the quantized vibrational frequencies ω_{lp} and wave vector values ξ_{lp}/R for the particle with radius R from the relation

$$\omega_{lp}=\frac{\xi_{lp}}{R}v_l. \tag{13}$$

For a free particle, α is given by the ratio of the transverse and longitudinal sound velocities v_t/v_l in the particle. In the case of an embedded particle, α additionally depends on the sound velocities in the matrix and on the ratio of mass density of particle to matrix. Furthermore, α is complex due to sound emission into the matrix and therefore the particle vibrations are damped.[17]

In order to derive the Raman scattering efficiency, we have to consider the interaction between the electrons and acoustic phonons. The Raman scattering is caused by fluctuations in the dielectric susceptibility, produced by the strain waves. They can be expressed as a function of the elasto-optic coefficients.[23,24] The wave vector dependence of the Raman scattering cross section of an acoustic mode is given by

$$\frac{d\sigma}{d\Omega}\sim(n+1)q\left[\int_V\exp[-i(\boldsymbol{k}^S-\boldsymbol{k}^L-\boldsymbol{q})\boldsymbol{r}]dV\right]^2$$
$$\sim(n+1)q\,\delta(\boldsymbol{k}^S-\boldsymbol{k}^L-\boldsymbol{q}), \tag{14}$$

provided that the dimension of the scattering volume is large compared to $1/q$. The parameter $n=[\exp[(\hbar\omega)/(kT)]-1]^{-1}$ is the Bose–Einstein population factor.

The delta function in Eq. (14) expresses the momentum conservation in bulk crystals: The wave vectors of the scattered light $\boldsymbol{k}^S$ and of the exciting light $\boldsymbol{k}^L$ are very small. Therefore, only phonon excitations with wave vectors $\boldsymbol{q}=\boldsymbol{k}^S-\boldsymbol{k}^L$ near the center of the first Brillouin zone are allowed. For nanoparticles, the integral in Eq. (14) is limited by the sphere volume of radius R. Consequently, the delta function should be replaced by the scattering function $S(q,R)$. The wave vector selection rules are relaxed and Raman scattering by phonons of larger wave vectors is possible. Further, we take into account a low-frequency density of states $\sim q^2$. For spherical particles surrounded by an elastic matrix, the elastic excitations are damped according to $\exp(-b_it/2)$, the eigenvalues ξ are complex and the eigenmode with index i has a Lorentzian frequency distribution

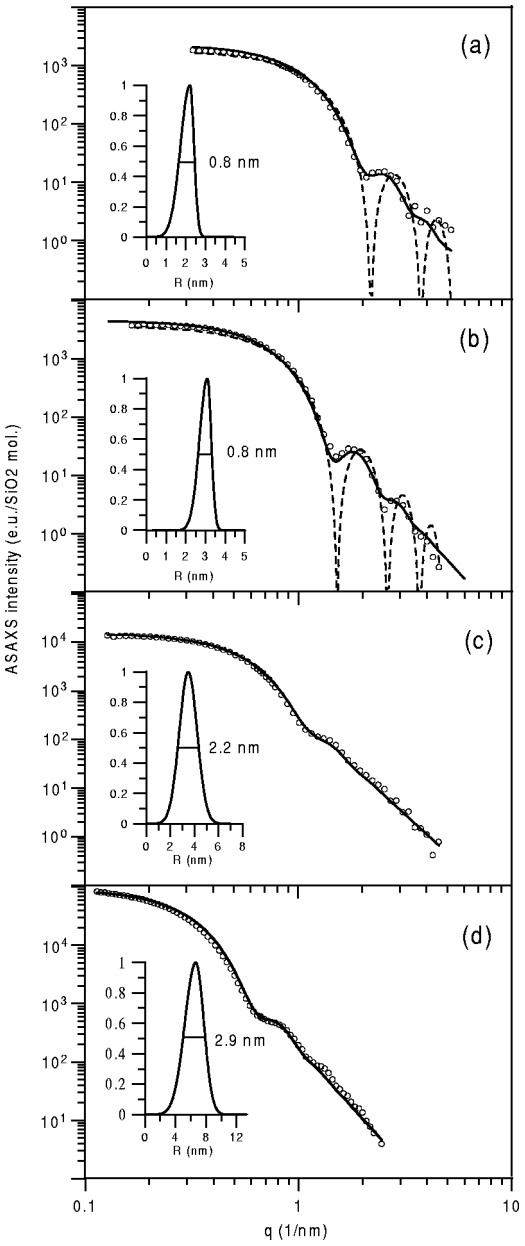

FIG. 1. Scattering curves of the samples (a) OG530, (b) OG550, (c) OG590, and (d) RG665. The excitation energy was 9.46 keV. The solid line has been fitted assuming spherically shaped particles with asymmetric size distribution as shown in the inset. The dashed line represents the scattering curve neglecting the size distribution.

TABLE II. Results obtained from least-squares fits of the measured scattering curves with different size distribution functions: log-normal (l-n), Gaussian (G), modified Gaussian (mG), and Lifshitz-Slezov (LS). R_0 and b denote the maximum and halfwidth of the size distribution $c(R)$, respectively. The least-squares parameter χ^2 relates the fit result qualities for the different functions used.

	R_0 (nm)				b (nm)				χ^2			
	l-n	G	mG	LS	l-n	G	mG	LS	l-n	G	mG	LS
OG 530	2.06	2.05	2.22	2.24	0.62	0.70	0.81	0.83	3.33	3.16	2.92	2.82
OG 550	2.95	2.95	3.08	3.06	0.78	0.80	0.81	1.14	1.54	1.46	1.33	1.60
OG 590	3.50	3.50	3.63	3.98	1.52	1.75	2.20	1.48	1.75	1.48	1.30	1.95
RG 665	6.50	6.50	6.60	7.15	2.45	2.72	2.94	2.64	1.43	1.30	1.27	1.67

$L(\omega,\omega_i,b_i)\sim(1+[2(\omega-\omega_i)/b_i]^2)^{-1}$ with the maximum value at ω_i and the halfwidth b_i.

Considering the size distribution $c(R)$ we get the Raman scattering cross section for $q=\omega_{lp}/v_l$ as follows:

$$\frac{d\sigma_i}{d\Omega}\sim(n+1)\omega^3\int S(q,R)c(R)V(R)L(\omega,\omega_i,b_i)dR. \quad (15)$$

III. EXPERIMENTAL RESULTS AND DISCUSSION

The investigated samples were prepared from orange and red sharp-cut filter glasses. The commercial names of the filter glasses (obtained from Schott Glass Inc., Germany) are OG515, OG530, OG550, OG590, RG630, RG665, and RG695, where the number indicates the cutoff wavelength in nanometers. The cutoff wavelength depends on the size and the composition x of the CdS_xSe_{1-x} nanoparticles. The composition x was determined by Raman measurements of the LO phonon frequencies.[17] The sample thickness was prepared to about 100 μm, suitable for the x-ray transmission experiment.

The ASAXS measurements were performed at the beamline JUSIFA[25] at the Hamburg Synchrotron Laboratory. For calculations of contrast variation, four x-ray energies were used, three of which were below but close to the K-absorption edge of Se and the fourth one was much below the K-absorption edge at 9.64 keV. To get a wide range of scattering vectors q, the measurements were performed at two sample–detector distances.

Open circles in Fig. 1 show the experimental scattering curves for some of the samples measured with 9.64 keV radiation. Theoretical fits to the experimental scattering curves were obtained from Eq. (6) by using four different trial functions $c(R)$, defined as:

log–normal size distribution:

$$c(R)=(\sqrt{2\pi}\cdot R\sigma)^{-1}\exp[-\ln(R/R_0)^2/(2\sigma^2)], \quad (16)$$

Gaussian size distribution:

$$c(R)=(\sqrt{2\pi}\cdot\sigma)^{-1}\exp[-(R-R_0)^2/(2\sigma^2)], \quad (17)$$

modified Gaussian (asymmetric) size distribution:

$$c(R)=\frac{2}{\sqrt{2\pi}(\sigma_1+\sigma_2)}\cdot\begin{cases}\exp[-(R-R_0)^2/(2\sigma_1^2)] & \text{for } R\leqslant R_0\\ \exp[-(R-R_0)^2/(2\sigma_2^2)] & \text{for } R>R_0,\end{cases} \quad (18)$$

and Lifshitz–Slyozov size distribution[26]

$$c(u)=\begin{cases}\dfrac{3^4\cdot\exp[(2u/3-1)^{-1}]}{2^{5/3}\cdot(u+3)^{7/3}(3/2-u)^{11/3}} & \text{for } u<1.5\\ 0 \quad \text{for } u>1.5\end{cases} \quad (19)$$

with $u=R/R_0$. The applied nonlinear least squares fitting method was based on the Levenberg–Marquardt algorithm. The Lifshitz–Slyozov function was derived theoretically[23] for describing the size distribution of crystallites grown under conditions of thermodynamic equilibrium. This function has an asymmetric shape with a pronounced tail towards low radii. However, it contains only one free adjustable parameter yielding poor fit results in comparison to the other functions used. Simple functions with two adjustable parameters often used to describe size distributions are the Gaussian and the log–normal functions. The minimized sum χ^2 of the squares of the deviations of the theoretical curves from the experimental points was smaller for the symmetric Gaussian than for the asymmetric log–normal function, which always has a pronounced tail for larger particles. To have free adjustable parameters for both tails we have used, therefore, a function defined by Eq. (18) and found smallest χ^2 values for distributions with a tail extending toward smaller particles. The final fitting curves are presented by solid lines in Fig. 1. The estimated mean radii are listed in Table II.

However, according to Table II the mean particle size obtained is not very sensitive to the fit function used. As an example, Fig. 2 shows the best fit results for the sample OG550 for all four trial functions.

Figure 3 shows the F_p' dependence of the square root of the normalized scattering cross section at $q=0$ for some selected samples. The full circles and the straight lines indicate the experimental values at four x-ray energies used and the corresponding linear least square fit, respectively. The ratio η of the molecule densities in the particle and the matrix phase were obtained from the slope of the fitted curves in Fig. 3. The results are given in Table III. For comparison η was also calculated using the molecular weights and densities according to the chemical composition. Since the molecule density in the particle phase changes by only 8% in the

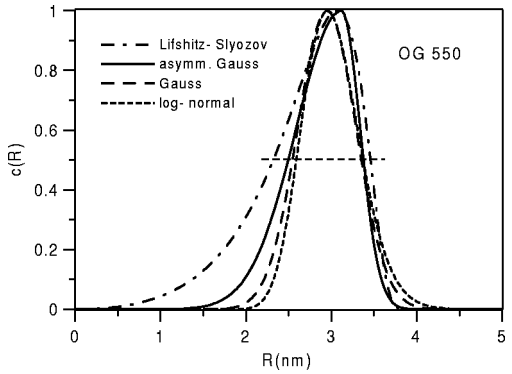

FIG. 2. Size distribution curves from fits with different model functions based on the assumption of spherically shaped particles.

compositional range of $x=0.2-0.67$, the range $\eta=0.7-0.79$ is realistic due to different densities of the glass matrix.

To obtain the volume fraction v_f of the particles, the scattering curves versus the scattering vector q, measured at $E=9.64$ keV, were integrated numerically. The values v_f were calculated using Eq. (10) and are given in Table III. The volume fraction was also calculated independently from the measured scattering cross section at $q=0$ using Eq. (11) and are also listed in Table III. Obviously, the values of v_f derived by the two methods agree well. For sharp size distributions, the factor A in Eq. (11) is only weakly dependent on the choice of the size distribution. For example, values of A are calculated for Gaussian and log–normal size distributions as a function of the relative halfwidth b/R_0 and are shown in Fig. 4. The values v_f in the last column of Table III are the mean values obtained for the four different x-ray energies.

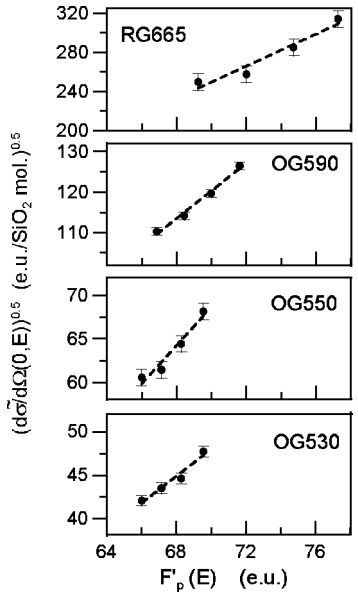

FIG. 3. Contrast variation measurements. The scattering intensities from ASAXS measurements were extrapolated to $q=0$. The x-ray energies 12.511, 12.652, and 12.658 keV are close to the K-absorption edge of Se and 9.486 keV is much below the absorption edge. The cross section is given in electron units/SiO_2 molecule. $F'_p(E)$ is given in electron units.

TABLE III. Molecular densities η and volume fractions v_f of the nanoparticles obtained by contrast variation.

	x	η	v_f Eq. (10)	v_f Eq. (11)
OG 530	0.67	0.79	0.0034	0.0038
OG 550	0.67	0.79	0.0025	0.0027
OG 590	0.55	0.87	0.0024	0.0031
OG 665	0.20	0.70	0.0043	0.0045

Next, we compare the particle radii obtained from ASAXS measurements with those obtained from Raman measurements on identical samples. The details of the Raman measurements have been discussed elsewhere.[17] As an example, low-frequency Raman measurements of sample OG 550 are represented in Fig. 5. The spectrum of the base material [curve (a)] containing no semiconducting nanoparticles shows a broad structure centered at about 50 cm^{-1}. This structure is known as the Boson peak[6,18,19] and is attributed to vibrations of the glass matrix.

The nanoparticle spectra in curves (b) and (c) are superimposed on this spectrum. They were measured in the depolarized and polarized configurations, respectively, after heat treatment of the glass.

The strongest peaks in curve (b), indicated by ω_{21}, and in curve (c), indicated by ω_{01}, are attributed to the $l=2$ and $l=0$ fundamental vibrations, respectively. The weaker peaks in curve (c) are some overtones of the $l=0$ mode and of the depolarized mode ω_{21}, which is allowed in the polarized configuration too. The weaker peak in curve (b) is found at the calculated position of the first overtone of the $l=2$ mode. Although the $l=0$ modes are not allowed in the depolarized configuration, an overlap with a small component of the strong $l=0$ mode ω_{01} cannot be excluded due to either experimental misalignment or due to deviations from the spherical shape of the particles.

First, we consider the measured total symmetric modes ω_{01}. A simple way to get the mean particle radii R_0 is to calculate them with Eq. (13) using the observed peak maximum for ω. The radii obtained in this way are given in the last column of Table IV.

In comparison to the ASAXS measurements, the results obtained from Eq. (13) give larger values of particle radii for

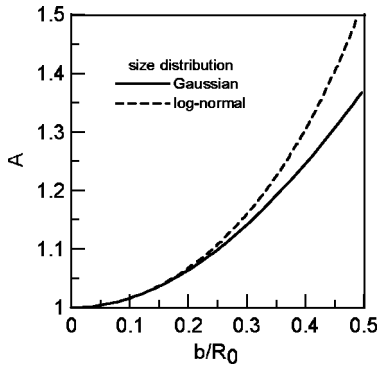

FIG. 4. Function A defined in Eq. (9) for Gaussian and log–normal size distribution.

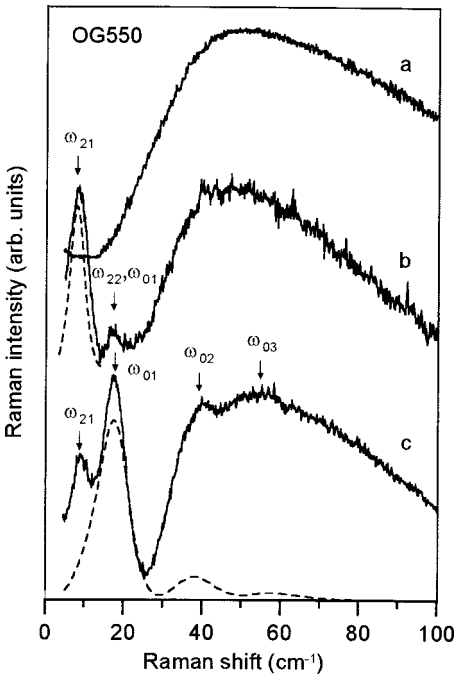

FIG. 5. Low frequency Raman scattering spectra of sample OG550, excited with $\lambda = 850$ nm: (a) unpolarized spectrum of the base glass before heat treatment, (b) depolarized spectrum of OG550, (c) polarized spectrum of OG550. The arrows show the spherically symmetric ω_{01} and the quadrupolar symmetric ω_{21} acoustic vibration and some overtones ω_{02}, ω_{03}, and ω_{22}. The dashed curves were fitted using Eq. (15).

all samples. In the case of size-distributed particles, large particles contribute much more than smaller ones to the Raman scattering cross section, which is proportional to the particle volume. As a result, the maxima of the Raman modes correspond to larger radii than the mean radius R_0. Therefore, for a more refined comparison between results of ASAXS and Raman scattering experiments and theory, we used Eq. (15) for the Raman scattering efficiency. Gaussian particle size distribution functions were used with the parameter σ taken from the results of the ASAXS measurements. The damping parameters of the confined acoustic modes caused by influence of the glass matrix on the particles were taken from Ref. 17. The particle radii obtained from the best fit to Raman spectra, listed in Table IV, are in good agreement with the ASAXS values. As pointed out in Sec. II,

TABLE IV. Particle radii, obtained from ASAXS and Raman measurements. The values in the last row were calculated from Eq. (13) assuming that the observed Raman shift of the $l=0$ and $p=1$ mode is identical with the vibrational frequency ω.

	R_0 (nm) ASAXS	R_0 (nm) Raman	R_0 (nm) Eq. (13)
OG 515	2.16	1.98	2.17
OG 530	2.22	2.00	2.22
OG 550	3.08	3.25	3.65
OG 590	3.63	3.68	4.42
OG 665	6.65	6.70	7.78
RG 630	2.90	2.76	3.40
RG 695	4.20	4.33	5.38

TABLE V. Halfwidths of the confined acoustic mode ω_{01}: b_{ex} is the experimental value obtained from Raman spectra in Ref. 17, b_{th} is obtained theoretically from Eq. (15), based on the measured Gaussian size distribution (parameters in Table II), and b_0 is the calculated acoustic mode damping of particles with radius R_0, embedded in glass Ref. 17.

	b_{ex} (cm^{-1})	b_{th} (cm^{-1})	b_0 (cm^{-1})
OG 530	9.7	17.2	13.1
OG 550	8.7	9.3	8.0
OG 590	8.2	9.5	6.3
OG 665	4.8	4.7	3.3

small angle scattering is sensitive to density differences between particle and matrix. The size of the particles obtained by ASAXS experiments is not necessarily the actual size of the crystalline core of the particles. In order to distinguish whether the particle is completely crystalline or amorphous, wide angle scattering to detect Bragg peaks could be used, as already applied to PbSe quantum dots by Lipovskii *et al.*[27] However, the Raman spectra of the optical phonons of the CdS_xSe_{1-x} nanoparticles[17] could be clearly assigned to the crystalline phase.

Particle size distribution is one reason for broadening of the Raman peaks. The peaks are further broadened by damping of the confined acoustic modes because the particles are embedded in the glass matrix. The corresponding damping parameters b_0, obtained from the imaginary parts of the eigenfrequencies of the acoustic modes for particle radius R_0, are given in Table V. The resulting theoretical halfwidths b_{th} of the confined acoustic phonons were calculated with Eq. (15), using b_0 and a Gaussian size distribution with the parameters given in Table II. Except for sample OG 530 containing the smallest particles, the calculated halfwidths b_{th} agree with the measured halfwidths b_{ex}, as seen from Table V. The calculated phonon widths would be reduced assuming incomplete elastic coupling of the particles with the surrounding matrix, reducing the halfwidth b_0. This could be true for very small particles and imperfect spherical shape.

The dashed curves in Fig. 5 were fitted using Eq. (15). The measured Raman scattering intensities of different samples were normalized to their Raman scattering intensities of the Boson peak of the glass matrix and to the volume fraction v_f determined by the ASAXS measurements. Figure 6 shows the dependence of the normalized Raman scattering cross section (open circles) on the mean particle radius for the $l=0$ mode. This dependence corresponds well with the solid line which was calculated using Eq. (15).

IV. CONCLUSIONS

Size and size distribution of CdS_xSe_{1-x} nanocrystallites embedded in a silicate glass matrix were investigated by ASAXS measurements. Mean radii between 2 and 7 nm were measured in the samples with different composition and heat treatment. Best fit results for the size distribution were obtained with asymmetric functions showing a slightly enhanced tail toward smaller particles, which is also theoretically predicted for nanoparticles formed as a result of a coa-

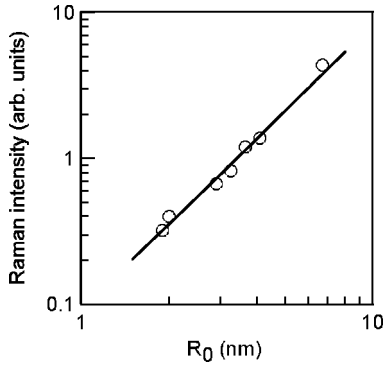

FIG. 6. Measured Raman scattering intensity (circles) of the acoustic mode ω_{01} with index $l=0$ in dependence on the mean particle radius. The intensity was normalized to the Raman scattering intensity of the Boson peak of glass and to the volume fraction v_f. The solid curve indicates the theoretical dependence on the mean particle radius and was calculated using Eq. (15).

lescence process during the heat treatment. The mean radii calculated from the ASAXS measurements agree well with those measured by low-frequency Raman scattering. For the larger particles, deviations of the radii determined by the two methods are smaller than 5%. Larger deviations for smaller particles could be due to the stronger confinement, restricted applicability of the continuum theory, and a nonlinear dispersion curve. The peak frequency and the halfwidth of the Raman bands depend on the particle size distribution as well as on the acoustic mode damping due to a particle–matrix effect. The observed halfwidths are smaller than the calculated ones assuming the perfect contact between particle and matrix. This could be an indication of incomplete elastic coupling at the interface. By contrast variation using four different x-ray energies, the ratio of molecular densities in the particles, and the surrounding matrix could be determined. Additionally, the particles volume fraction was obtained.

[1] U. Woggon, *Optical Properties of Semiconducting Quantum Dots* (Springer, Berlin, 1997).
[2] B. Champagnon, B. Andrianasolo, A. Ramos, M. Gandais, M. Allais, and J.-P. Benoit, J. Appl. Phys. **73**, 2775 (1993).
[3] M. P. A. Müller, U. Lembke, U. Woggon, and I. Rückmann, J. Non-Cryst. Solids **144**, 240 (1992).
[4] G. Goerigk, H.-G. Haubold, C. Klingshirn, and A. Uhrig, J. Appl. Crystallogr. **27**, 907 (1994).
[5] A. Boukenter, B. Champagnon, E. Duval, J. L. Rousset, J. Dumas, and J. Serughetti, J. Phys. C **21**, L1097 (1988).
[6] V. K. Malinovsky, V. N. Novikov, A. P. Sokolov, and V. C. Dodonov, Solid State Commun. **67**, 725 (1988).
[7] H. B. Abel, Phys. Status Solidi B **161**, 435 (1990).
[8] B. Champagnon, B. Andrianasolo, and E. Duval, J. Chem. Phys. **94**, 5237 (1991).
[9] J. A. Capobianco, P. P. Proulx, B. Andrianasolo, and B. Champagnon, Phys. Rev. B **43**, 10031 (1991).
[10] M. Fujii, T. Nagareda, S. Hayashi, and K. Yamamoto, Phys. Rev. B **44**, 6243 (1991).
[11] A. Tanaka, S. Onari, and T. Arai, Phys. Rev. B **47**, 1247 (1993).
[12] M. Montagna and R. Dusi, Phys. Rev. B **52**, 10080 (1995).
[13] T. Bischof, M. Ivanda, G. Lermann, A. Materny, and W. Kiefer, J. Raman Spectrosc. **27**, 297 (1996).
[14] M. Rajalakshmi, T. Sakuntala, and A. K. Arora, J. Phys.: Condens. Matter **9**, 9745 (1997).
[15] A. Roy and A. K. Sood, Solid State Commun. **97**, 97 (1996).
[16] L. Saviot, B. Champagnon, E. Duval, and A. I. Ekimov, Phys. Rev. B **57**, 341 (1998).
[17] P. Verma, W. Cordts, G. Irmer, and J. Monecke, Phys. Rev. B **60**, 5778 (1999).
[18] V. K. Malinovsky and A. P. Sokolov, Solid State Commun. **57**, 757 (1986).
[19] A. P. Sokolov, A. Kistiuk, D. Quitmann, and E. Duval, Phys. Rev. B **48**, 7692 (1993).
[20] A. Guinier and G. Fournet, *Small-Angle Scattering of X-rays* (Wiley, New York, 1955).
[21] E. Duval, Phys. Rev. B **46**, 5795 (1992).
[22] A. Tamura, K. Higata, and T. Ichinokawa, J. Phys. C **15**, 4975 (1982).
[23] A. Pinczuk and E. Burstein, in *Light Scattering in Solids I*, edited by M. Cardona (Springer, Berlin, 1983), p. 23.
[24] M. Cardona, in *Light Scattering in Solids II*, edited by M. Cardona and G. Güntherodt (Springer, Berlin, 1982), p. 19.
[25] H.-G. Haubold *et al.*, Rev. Sci. Instrum. **60**, 1943 (1989).
[26] I. M. Lifshitz and V. V. Slyozov, J. Phys. Chem. Solids **19**, 35 (1961).
[27] A. Lipovskii *et al.*, Appl. Phys. Lett. **71**, 3406 (1997).